LHCb note 2003-015

Silicon Tracker simulation performance.

Matthew Needham
Physik-Institut der Universität Zürich

February 13, 2003

Abstract

The simulation of the LHCb Silicon tracker is described and the resulting performance discussed

1 Introduction

The LHCb Silicon Tracker (ST) project consists of two sub-detectors that will be built using silicon micro-strip technology. The first is the so-called 'Trigger Tracker' (TT). This consists of four layers of silicon located in two distinct 'half-stations' upstream of the magnet (Fig. 1). In Fig. 2 the layout of a layer in TT is shown. It is proposed to build this station using silicon of 500 μm thickness with ladders ranging in length from 11 to 33 cm. The second sub-detector is the inner part of the main tracker. The 'Inner Tracker' (IT) will cover a cross-shaped area around the beam-pipe in each of the three tracking stations. An IT station will consist of four independent boxes arranged around the beam-pipe (Fig. 3). Each box will contain four layers of 300 μm thick silicon arranged in 11 and 22 cm long ladders.

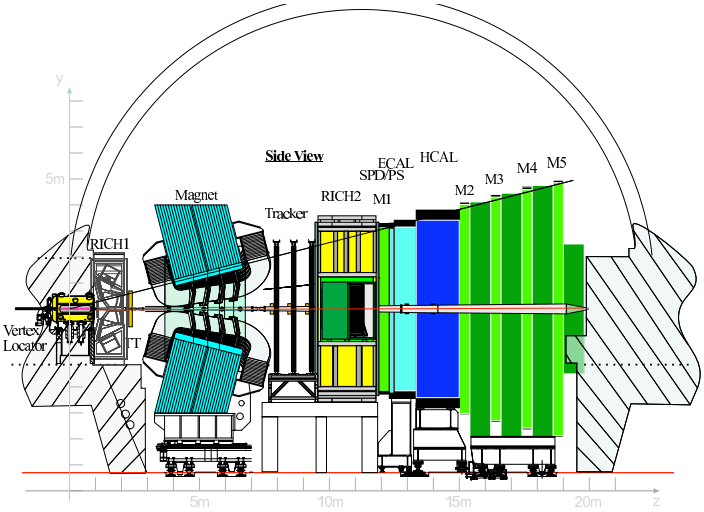

Figure 1: Sideview of the LHCb detector.

In the first half of this note the simulation and digitization of the detector are described in detail. It should be noted that the IT and TT sub-detectors are very similar in nature and described by a common set of software. Where parameters are different this is driven by data cards.

In the second-half of the note the performance of both sub-detectors is described. Numbers for detector occupancies updating those given in [1] are presented. Finally the performance of the sub-detector reconstruction — the clustering is described.

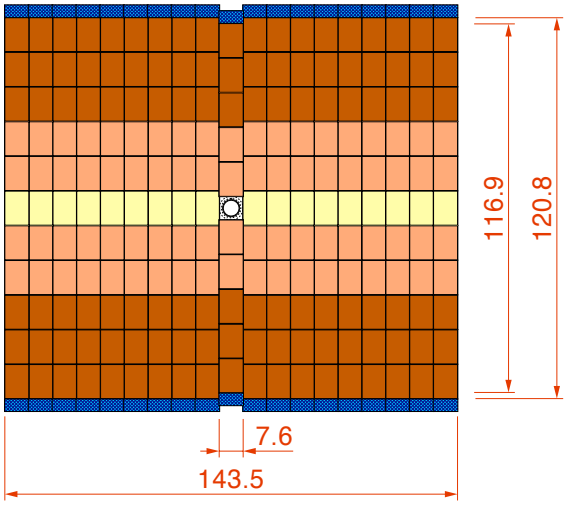

Figure 2: Layout of TT layer 1.

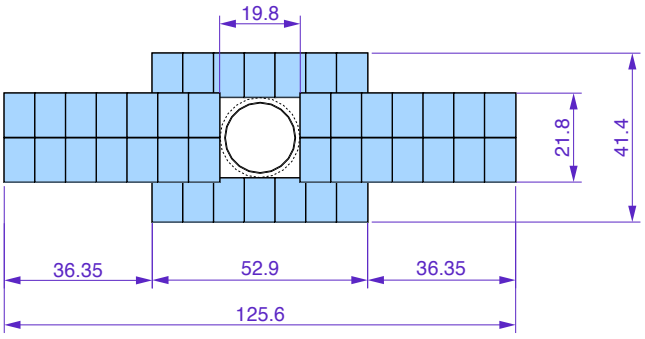

Figure 3: Layout of IT2.

2 GEANT3 simulation

The simulation of the ST is currently performed within the LHCb GEANT3 based simulation package SICBMC [2]. The geometry implemented [3] includes not only the 'sensitive' area of the silicon but also the various dead detector elements within the experimental acceptance.

The sensitive elements of the detector are described in detail and match the layouts proposed in [4] and [5]. Detector overlaps and the staggering of the z positions of wafers are implemented (Fig. 4), as well as individually rotated

ladders in the stereo-layers. At the simulation level the whole surface of a ladder is assumed to be sensitive. However, during the digitization step the additional insensitive area due to the guard-rings is correctly simulated. The material of the carbon fibre supports has not been explicitly simulated. Instead, it has been accounted for by increasing the thickness of the silicon in IT from 320 μm to 400 μm and the silicon in TT from 500 μm to 600 μm.

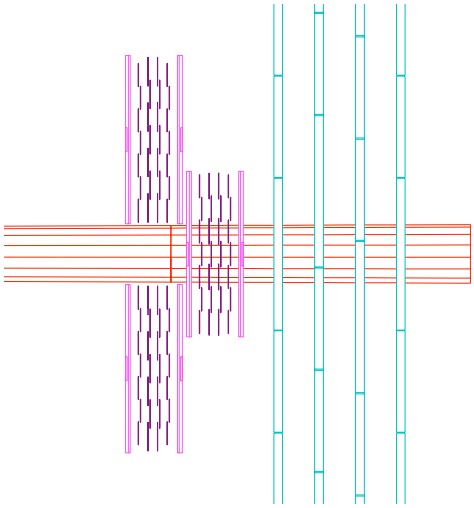

Figure 4: GEANT layout of wafers in an IT station.

A simplified description of the insensitive detector material is used in order to speed up the simulation. In the case of the IT stations the dead material of each detector box is described by several rectangular regions positioned upstream and downstream of the sensitive detector area (Fig. 5). These simulate the box walls, the front-end electronics and hybrids, the balconies, cooling plate and patch panel. In each case the radiation and interaction length used have been tuned to give the currently estimated average values. Support beams and cables running to the outer frames of the detector are simulated in a similar way. The values used in the various regions are summarized in Table 1. The dead material of the TT station is described in a similar way. However, it should be noted that in this case most of the dead material lies outside the experimental acceptance and therefore has no impact on the performance of the detector.

The output of the GEANT step for each sub-detector is a ZEBRA bank. In the case of the ST this contains for each particle the point at which it

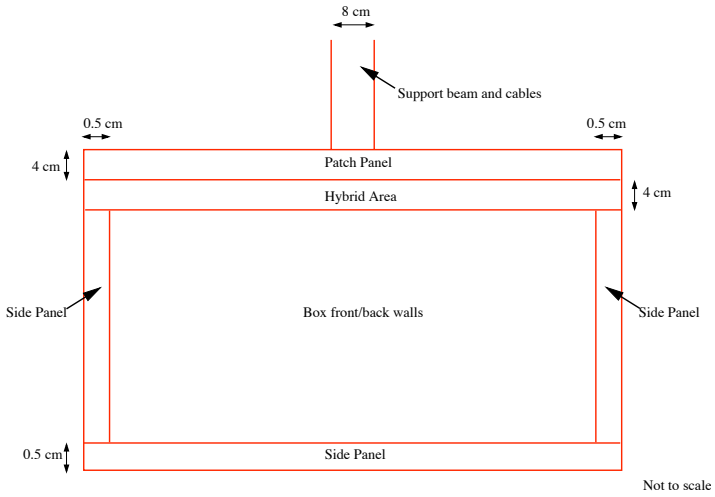

Figure 5: IT frames and dead material (x-y view).

Region	Thickness/cm	X_0/cm	λ_I/cm
Box front/back walls	2×0.068	32.000	55.7
Box side walls	2×0.48	32.000	55.7
Hybrid Area	2×0.55	13.8	44.2
Patch Panel	2×0.33	13.8	44.2
Support frames/cables	2×0.18	8.89	39.0

Table 1: IT Detector frame parameters.

entered and exited each layer of the detector, the energy deposited in the layer and the time-of-flight. This information forms the input to the Object Orientated digitization software.

3 Digitization Procedure

The digitization step is implemented within the Gaudi framework [6] and currently runs within the LHCb reconstruction program Brunel [7]. A more detailed description of the data model and algorithms can be found in [8]. The digitization proceeds as shown in Fig. 6:

- The MCHits (from GEANT) are converted to MCITDeposits. In this step the charge deposited on each detector strip is calculated taking

into account the track angle, charge sharing and the sampling time.

- All MCITDeposits related to one channel are grouped together to give MCITDigits.
- The MCITDigits are converted to ITDigits. During this stage inefficiency due to dead strips is allowed for and detector noise is added.

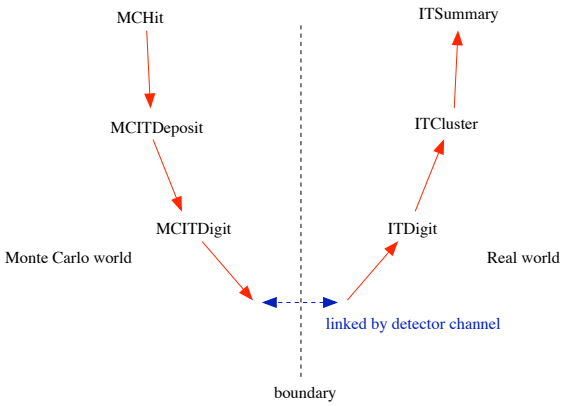

Figure 6: Silicon tracker data model.

The features of the digitization that use input from test-beam and other measurements on prototype sensors are described below.

3.1 Charge deposition

The charge deposited on a strip by a particle traversing a silicon sensor is calculated as follows. First, the trajectory of the particle through the sensor is calculated as a straight line connecting the entrance point to exit point of the MCHit. Charge is then generated along the trajectory at sites spaced by 20 μm along the measurement coordinate of the sensor. A constant charge density is assumed. The total generated charge is sampled from a Landau distribution that is convolved with a Gaussian to account for atomic binding effects. The values of the parameters currently used are given in Table 2.

The charge on each site is then distributed between readout strips using the charge sharing model shown in Fig. 7. This is based on data taken during the June 2002 test-beam with a 90V bias voltage [9]. Finally, the test-beam data exhibit 'shoulders' [9]. This effect is most likely attributable to capacitive

Parameter	TT value/e^-	IT value/e^-
Mean of Landau	34000	24000
Landau width	1400	1400
σ of Gaussian	1700	1700

Table 2: Charge deposition parameters.

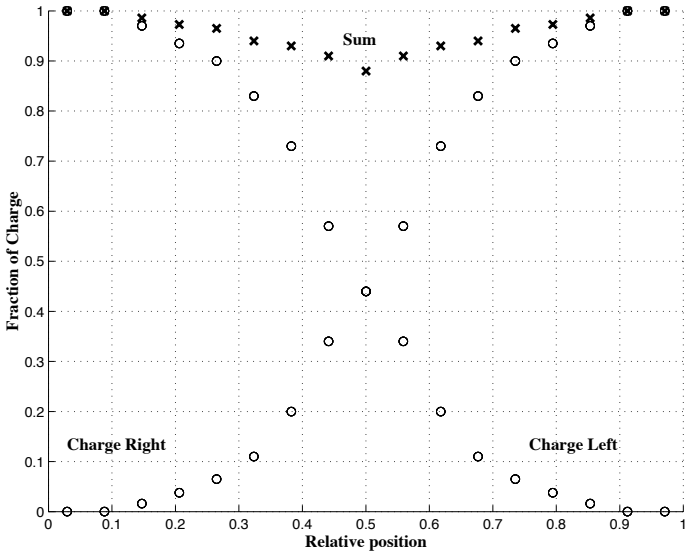

Figure 7: Charge sharing model. This is implemented in the simulation as a look-up-table.

coupling between the strips. It is simulated by re-distributing the charge on each strip according to the model shown in Fig. 8. A value of δ of 0.11, obtained from the data is used.

3.2 Spillover

The time between bunch collisions at the LHC will be 25 ns which is comparable with the shaping time of the readout amplifier. The signals shapes used in the digitization for the IT and TT detectors are shown in Fig. 9. Both curves are based on test-pulse measurements made with the front-end chip — the Beetle that will be used in the ST [10]. The distribution for the TT stations is broader than that for the IT stations due to the increased

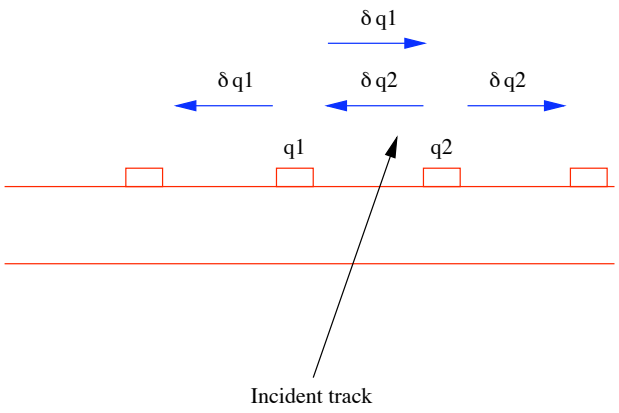

Figure 8: Model of capacitive coupling between the strips.

capacitive load. It can be seen from Fig. 9 that particles originating in the

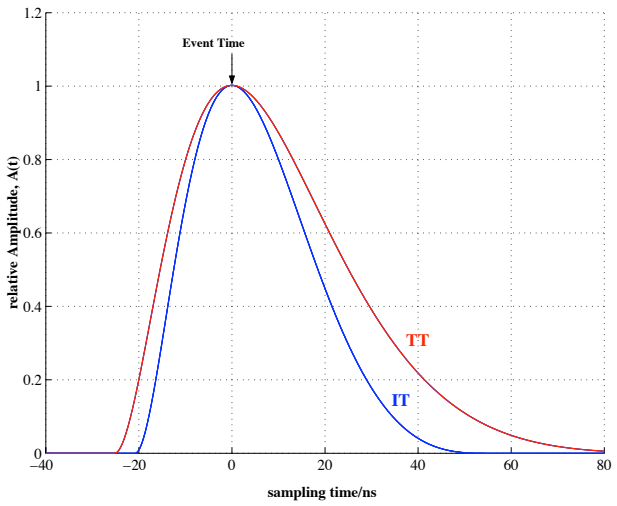

Figure 9: Amplifier response.

two crossings prior to the triggered event can give a significant signal. In addition there will also be a contribution due to low energy secondary particles generated in the previous crossings that give hits in the detector around the event time. These two effects are referred to as 'spillover' and are treated in the following way. If t_f is the time-of-flight calculated by GEANT of the particle to the detector plane and t_{spill} is the 'spill time' relative to the triggered event then the collected charge q_c is given by:

$$q_c = q \times A(t_{off} - t_f - t_{spill})$$

where A(t) is determined from Fig. 9 and t_{off} is the time-of-flight of relativistic pions and calculated for each of the stations separately.

3.3 Detector inefficiency and noise

The final step of the digitization is to allow for detector inefficiency and the noise of the front-end electronics. It is currently assumed that 1 % of channels, randomly distributed in the detector will be dead for one reason or another.

To simulate the noise due to the front-end electronics the following procedure is adopted. For each strip hit by a real particle the total charge is smeared by a Gaussian distribution. The width of the Gaussian is obtained from measurements of the Beetle performance [10]. The values used are summarized in Table 3. In addition, for each event a constant fraction of random

Sub-detector/e^-	Value/e^-
TT	2700
IT	2000

Table 3: Noise levels assumed in TT and IT. In both cases they correspond to a S/N ratio of 12.

noise strips are generated with a charge sampled from the tail of a Gaussian distribution. In this way the effect of noise clusters is properly simulated without having to generate a signal in every channel of the detector. To be consistent with the clustering algorithm described in Section 4.2 the fraction of noise strips is set to 1.35×10^{-3} and the minimum generated charge set so that it corresponds to a S/N of 3.

4 Performance

The performance studies were done using data produced with SICBMC v259r0 and dbase v253r0. For the reconstruction Brunel v16r4 and XmlDDDB version v14r0 were used. The quoted results are for a sample of 5000 $B_d \rightarrow J/\psi(\mu^+\mu^-)K_S(\pi^+\pi^-)$ events. A luminosity from the machine of 2×10^{32} cm^{-2}s^{-1} was assumed and spillover from the bunch crossings at -50, -25 ns considered.

4.1 Occupancies

Occupancies in the ST station were discussed in [1]. Since that time a number of changes have taken place that effect the numbers presented there:

- Random noise hits are now generated. This increases the occupancy by $\sim 1 \times 10^{-3}$.
- The pitch of the detector has decreased from 240 μm to 200 μm. This decreases the occupancy by a relative factor of 0.8.
- The charge sharing model has been updated. Compared to [11] the charge loss in the inter-strip region is reduced. In addition the shoulders are now simulated. The net effect of these changes is to increase the occupancy by a factor of 1.2.
- Several small bugs have been found and fixed [12].
- The layout of the sensors in the TT station has been adjusted following the decision to construct this station entirely from silicon strip detectors.

As in [1] a channel is considered to be 'hit' if the deposited charge has a signal-to-noise ratio of 3. This value is chosen because in that case the channel will be considered in the clustering algorithm as described in Section 4.2.

4.1.1 TT occupancies

It can be seen from Fig. 2 that each of the four layers in the TT station can be sub-divided into five rows each of which is positioned at approximately constant y. Fig. 10 shows the occupancy in the first layer of TT-A. It can be seen that:

- The strips with the highest occupancy in each row are located around $x = 0$.
- The hottest region is in row 3 which is centred on $y = 0$. Here, an occupancy of $\sim 4\%$ is found.
- The occupancy falls rapidly with increasing distance from the beam-pipe.

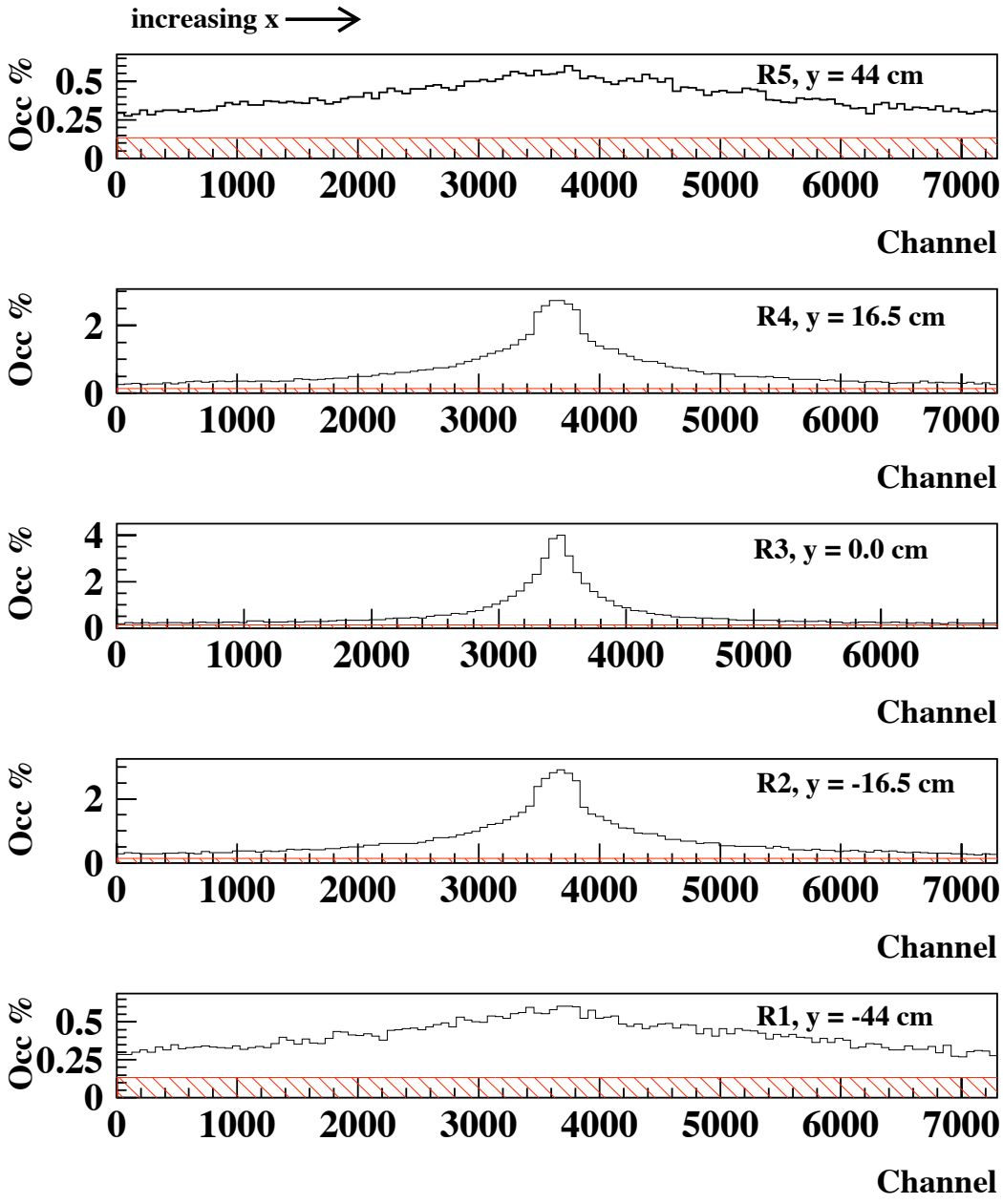

Figure 10: Occupancies in TT-A layer 1. The (red) hatched area is the occupancy contribution due to random noise.

The other layers in the TT station show a similar trend. Table 4 summarizes the occupancy in the hottest group of 64 strips in each TT row.

Row	Layer			
	TT-A,1	TT-A,2	TT-B,2	TT-B,2
1	0.6	0.6	0.6	0.7
2	2.9	2.7	2.6	2.8
3	4.0	4.1	4.0	4.0
4	2.7	2.6	2.5	2.7
5	0.6	0.6	0.6	0.6

Table 4: Maximum occupancy for each TT row in %.

4.1.2 IT occupancies

Table 5 summarizes the maximum and average occupancies in the inner tracker. The maximal occupancies are quoted for the hottest group of 64 strips in each box. Accounting for the changes discussed above these numbers are in good agreement with those presented in [1].

Station	Top/Bottom		Left/Right	
	max	av	max	av
1	0.5	0.4	1.6	0.7
2	0.4	0.4	1.6	0.7
3	0.4	0.3	1.5	0.6

Table 5: Maximum and Average occupancies in the IT stations in %.

4.2 Clustering

Due to the large strip pitch used in the ST the majority of clusters are expected to consist of one or two strips. Therefore, a simple clustering algorithm is sufficient. The ITDigits are first ordered by channel. A loop is

then made until an ITDigit above a S/N threshold is found. This is then taken as a cluster candidate. If the subsequent ITDigit is above threshold and is in the adjacent channel in the same sensor it is added to the cluster and so on. When the clustering procedure has stopped it is checked whether the total S/N of the cluster is above another threshold. Currently, the hit S/N threshold is set to 3 and the cluster S/N threshold is set to 3.2. This maximizes the efficiency of the clustering whilst still giving a tolerable rate of noise clusters. The effect of varying these cuts is discussed in Section 4.2.1. The cluster coordinate is determined from the charge weighted average of the strip coordinates. As in [11] a correction is applied to account for the non-linear charge-position dependence. With the addition of the 'shoulders' to the charge sharing model this correction has become less effective and further studies are needed to determine that this correction is still appropriate.

On average 463 clusters per event are produced in the TT station and 391 in the IT. It should be noted that there are large event-to-event fluctuations of these numbers. This can be seen from Fig. 11 in which the total number of clusters per event in the ST is plotted. Table 6 summarizes the relative contribution of spillover and noise clusters to these numbers. It can be seen

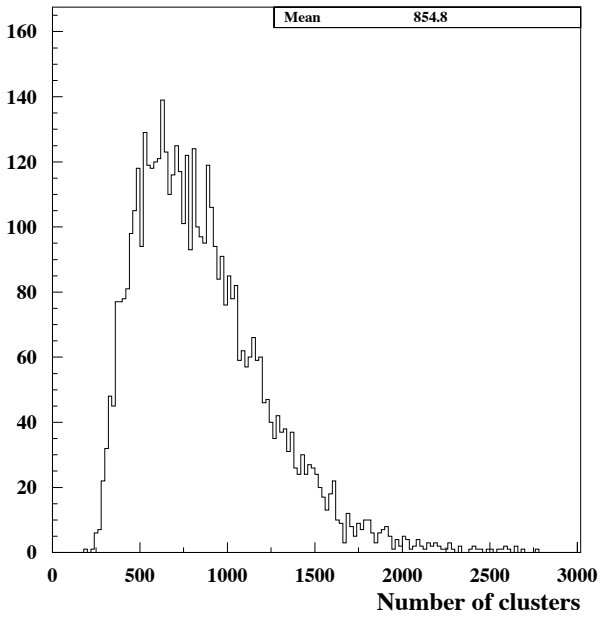

Figure 11: Number of clusters per event in ST.

Type	TT	IT
Spill, t = 0 ns	0.65	0.69
Spill, t= -25 ns	0.12	0.1
Spill, t= -50 ns	0.01	0.0
Noise	0.22	0.21

Table 6: Fractional contributions to the number of clusters.

that:

- $\sim$ 20% of the clusters are due to noise
- $\sim$ 10% of clusters are caused by particles produced in the crossings preceding the event.
- The TT stations are slightly more sensitive to spillover than the IT stations. This is expected due to the different front-end response (see Section 3.2).

Fig. 12 shows the distribution of cluster size. The average cluster size is 1.5. The tail out to large cluster sizes is due to high angle secondary tracks that hit many strips in the detector. It should be noted that the shoulders described in Section 3.1 have a noticeable impact on the clustering algorithm. If the simulation of the shoulders is switched off the average cluster size is reduced to 1.3.

4.2.1 Efficiency

The efficiency of the clustering procedure is defined as follows. First, particles are selected using Monte Carlo truth information that satisfy:

- $p > 1$ GeV
- $z_{origin} < 10$ cm

These requirements are necessary to remove low energy secondary particles which are not detected because they arrive in the detector much later than

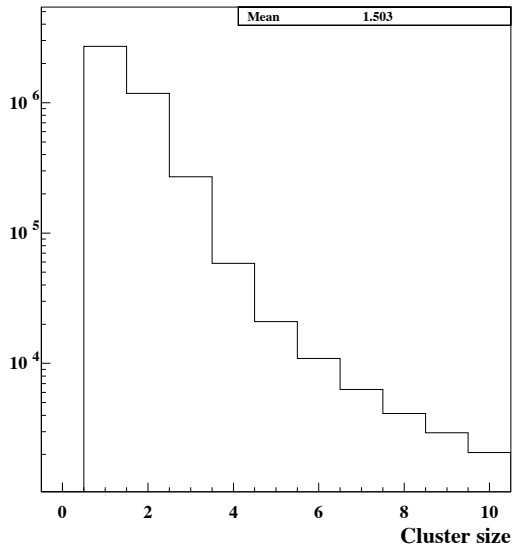

Figure 12: Distribution of cluster size.

the sampling time[1]. Then it is checked whether the particle went through each layer of the detector using the MCHit information from Geant. If this is the case at least one cluster should be reconstructed[2]. The efficiency of each layer is then:

$$\eta = \text{N(MC accepted)} \cap \text{at least one rec cluster)/N(MC accepted)}$$

This definition of efficiency seems natural since the track reconstruction expects that the ST provides on average close to one measurement per detector layer. However, it should be noted that this number can never be 100%. This is because as discussed in Section 2 the sensitive area of the detector as described in the GEANT simulation is larger than that considered at the digitization level.

Two sets of runs were made in which the cut on the cluster S/N was varied from 3 to 6. In the first set of runs the above definition of efficiency was used. In the second set particles passing through the outer guard rings of the detector were excluded from the determination of the efficiency (see Fig. 13). The results are shown in Fig 14 for a typical layer in:

[1]These particles have no physics interest.

[2]It can be more than one due to the overlap between wafers in a layer as shown in Fig 4.

- TT.
- a IT L/R box.
- a IT T/B box.

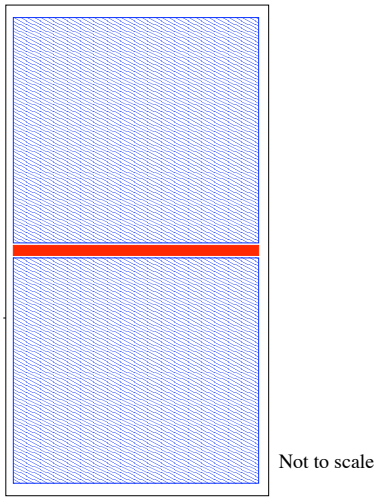

Figure 13: Layout of a two sensor ladder. In the first set of runs the entire surface of the wafer was considered in the efficiency determination. In the second set the hatched plus the solid area was considered. In the actual detector only the hatched area will be sensitive.

It can be seen that:

- The sensors in the T/B boxes have the highest efficiency. This because in these boxes only one sensor ladders are used.
- The efficiency of the L/R boxes is about 1% lower than the T/B boxes. This is due to the 2 mm dead region between the two sensors bonded to form one ladder.
- The efficiency of a TT is is also 1% lower than a T/B box. Again this is due to the dead regions between the sensors that are bonded together to form a ladder.
- In each case there is a small efficiency loss of around 0.5% as the cut on the S/N is varied from 3 to 6.

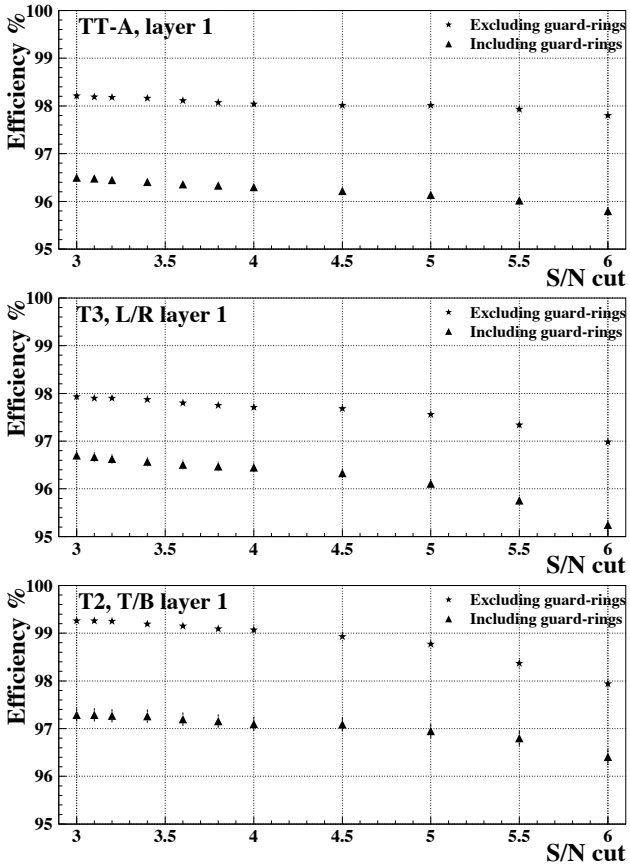

Figure 14: Clustering efficiency as a function of the cluster S/N cut.

Region	Efficiency % guard rings in	Efficiency % guard rings out
TT layer 1	96.5 ± 0.05	98.2 ± 0.04
IT L/R boxes	96.7 ± 0.1	97.9 ± 0.05
IT T/B boxes	97.3 ± 0.14	99.2 ± 0.08

Table 7: Layer efficiencies in % for the default simulation/reconstruction.

The efficiency numbers for the default S/N cut of 3.2 are given in Table. 7.

The effect of increased detector noise on the clustering efficiency has also been investigated. Fig. 15 shows the clustering efficiency as a function of

the S/N for the first layer in the T3 L/R boxes. As can be seen for S/N to noise values below 9.5 the efficiency starts to drop rapidly. This effect is also visible in the test-beam data [9]. It should also be noted that the track finding efficiency in the simulation is stable for clustering efficiencies as low as $\sim 92\%$ [13] which corresponds to a S/N of 7.

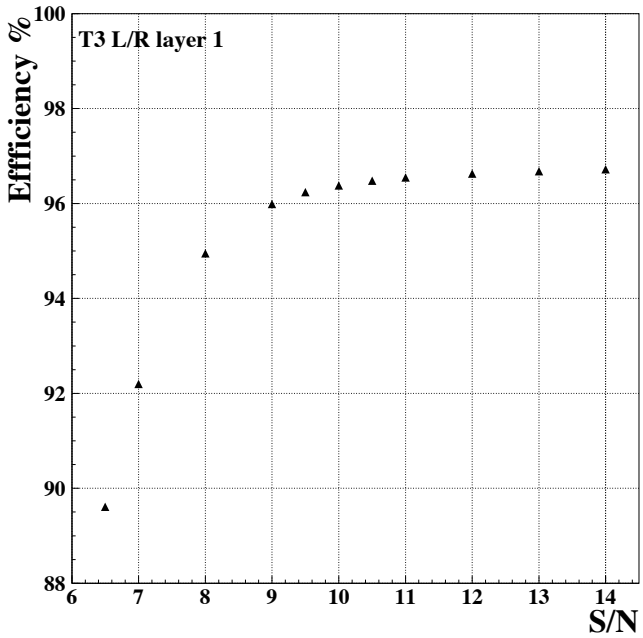

Figure 15: Clustering efficiency as a function of the detector S/N. A value of 12 is currently assumed in the simulation.

4.2.2 Resolutions

Fig.16 shows the obtained coordinate resolution for various cluster sizes. It can be seen that:

- None of the distributions are well described by Gaussian fits
- As expected the resolution for one strip clusters is roughly given by pitch/$\sqrt{12}$.

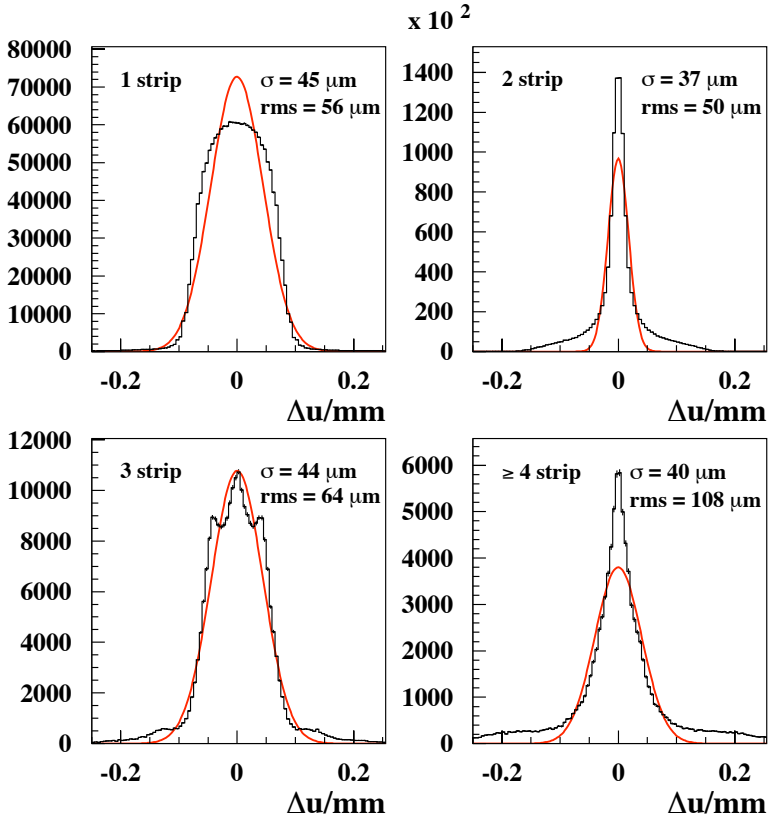

Figure 16: Cluster resolutions. The superimposed curves are the result of Gaussian fits.

- The shoulders degrade the resolution for two and three strips clusters noticeably and also give rise to the structure visible in three strip cluster distribution.

A Gaussian fit to the sum of the four distributions gives a resolution of 45 μm. This is in reasonable agreement with the value of 52 μm found in the test-beam data [9].

For the track fit [14] it is necessary for an estimate of the uncertainty on the reconstructed coordinate to be given for each cluster. Since none of the distributions are Gaussian it is not clear *a priori* what the optimal estimate of this uncertainty is. Currently, it is chosen to use the σ of the fitted Gaussians in Fig.16 as the estimator.

References

[1] M. Needham. Inner and outer tracker occupancies in the light LHCb detector. *LHCb-note*, (32), 2002.

[2] A. Tsaregorodtsev. SICB. http://lhcb.cern.ch/computing/sicb/html/sicbug.html, 1997.

[3] F. Ronga. Inner tracker geometry implementation in GEANT. *LHCb-note*, (106), 2000.

[4] The LHCb Collaboration. Inner Tracker Technical Design Report. CERN/LHCC 2002-029.

[5] O. Steinkamp. Ideas for all-silicon TT. LHCb note — in preparation.

[6] M. Cattaneo *et al.* GAUDI LHCb Data Processing Applications Framework User Guide. *LHCb-note*, 1999.

[7] M. Cattaneo *et al.* Brunel LHCb Reconstruction Program: User Guide. *LHCb-note*, 2001.

[8] M. Needham. New data model, digitization and reconstruction algorithms for the inner tracker. *LHCb-note*, (30), 2002.

[9] M. Agari *et al.* Test Beam Results of Multi-Geometry Prototype Sensors for the LHCb Inner Tracker. *LHCb-note*, (58), 2002.

[10] N. van Bakel *et al.* Performance of the Beetle Readout Chip for LHCb. Proc. 8th workshop on Electronics for LHC Experiments, Colmar France, September 9-13, 2002.

[11] A. Polouektov *et al.* First results from LHCb inner tracker performance studies using new digitization software. *LHCb-note*, (118), 2001.

[12] M. Needham. Inner Tracker Simulation Status. Talk at Cambridge LHCb Week 15/10/2002.

[13] The LHCb Collaboration. Status of the LHCb Detector Reoptimization. CERN-LHCC-003/LHC-H-023, 23^{rd} January 2003.

[14] M. Merk *et al.* Performance of the LHCb OO Track Fitting Software. *LHCb-note*, (86), 2000.